Calibration Report of the CIS Measurements in the Cluster Active Archive (CAA)

prepared by

I. Dandouras, A. Barthe, L. Kistler, A. Blagau

DOCUMENT STATUS SHEET

Issue	Date	Details
Version 1.0	30.01.2009	1st version, prepared for the CAA Peer Review. Document referenced as CAA-EST-CR-CIS.
Version 1.1	17.05.2010	Various updates, in preparation of the 5th CAA Operations Review.
Version 1.2	29.04.2011	Various updates, in preparation of the 6th CAA Operations Review.
Version 1.3	10.05.2012	Various updates, in preparation of the 7th CAA Operations Review.
Version 1.4	09.05.2013	Various updates, following the 2013 CIS-CAA Progress Meeting and in preparation of the 8th CAA Operations Review.
Version 1.5	12.05.2014	Various updates, in preparation of the 9th CAA Operations Review.
Version 1.6	29.10.2015	Various updates, in preparation of the 10th CAA Operations Review.
Version 1.7	15.05.2017	Various updates, in preparation of the 11th CAA Operations Review.

Table of Contents

Document Status Sheet 2
1 Introduction 4
2 Instrument Description 4
2.1 The CODIF (CIS-1) Instrument 5
2.2 The HIA (CIS-2) Instrument 5
3 Measurement Calibration Procedures 6
3.1 Calibration files 6
3.2 Detector efficiency 7
3.2.1 Determination of HIA efficiency 7
3.2.2 Determination of CODIF efficiency 8
4 Measurement Processing Procedures 10
5 Results of Calibration Activities 10
5.1 CODIF 10
5.1.1 H^+ efficiencies 11
5.1.2 O^+ efficiencies 11
5.1.3 Inter-anode comparisons 11
5.2 HIA 11
5.2.1 Inter-anode comparisons 12
5.2.2 Variation of HIA efficiency 12
6 Results of Cross-Calibration Activities 13
6.1 HIA efficiency 13
6.2 CODIF efficiency 13
6.3 HIA-CODIF Cross-Calibration 14
7 Summary 14
8 References 15

1 Introduction

The CIS (Cluster Ion Spectrometry) experiment, consisting of HIA and CODIF detectors, is a comprehensive ionic plasma spectrometry package onboard the four Cluster spacecraft, capable of obtaining full three-dimensional ion distributions (about 0 to 40 keV/e) with a time resolution of one spacecraft spin (4 sec) and with mass-per-charge composition determination (Rème et al., 2001).

The quality of the CIS data products is based on the calibration files that include:

- parameters determined during ground calibrations in vacuum test facilities and are stable through the mission,
- parameters that change gradually through the mission,
- parameters that can be changed during the mission by command.

All of them are equally important in converting raw data into physical units, and are used together.
The MCP particle detection efficiency degradation as a function of time is the single most important parameter to track and adjust during the mission. This includes total efficiency values, i.e. average response over the MCP surface, and anode cross-calibrations (relative efficiencies). Total efficiency evolution is evaluated by cross-calibrating the CIS provided densities with the density values provided by the Whisper sounder experiment. In addition CODIF provides also the time-of-flight performance statistics, which give a measure of the total efficiency evolution. Anode cross-calibrations are performed in gyrotropic plasma regimes.

An overview of these calibration procedures and their results is given in the present document.

2 Instrument Description

The CIS package consists of two different instruments:

- a time-of-flight ion *Composition and Distribution Function* analyser (*CODIF*, or *CIS-1*),
- a *Hot Ion Analyser* (*HIA*, or *CIS-2*).

In addition, each of the instruments, in order to be able to cover a dynamic range of about 7 orders of magnitude in particle fluxes, provides two different geometric factors: a *high-sensitivity side* (or *HS*) and a *low-sensitivity side* (or *LS*).

2.1 The CODIF (CIS-1) Instrument

The CODIF instrument combines ion energy per charge selection, by deflection in a rotationally symmetric toroidal electrostatic analyser, with a subsequent time-of-flight analysis after post-acceleration to ~15 keV/e. Ions are selected as a function of their *E/q* (energy per charge) ratio, by sweeping the high voltage applied between the two toroidal hemispheres. The full energy sweep with 31 contiguous energy channels is performed 32 times per spin. In the time-of-flight (TOF) section the velocity of the incoming ions is measured, which allows then the calculation of their *m/q* (mass per charge) ratio. Microchannel plate (MCP) electron multipliers are used to detect both the ions and the secondary electrons, which are emitted from a carbon foil at the entry of the TOF section, during the passage of the ions. These secondary electrons give the "start" signal, for the time-of-flight measurement, and the position information (elevation angle of the incoming ion, provided by the MCP sectoring in anodes), cf. Fig. 2.1.

In order to cover populations ranging from magnetosheath protons to tail lobe ions, a dynamic range of more than 10^5 is required. CODIF therefore consists of two sections, each with a 180° field of view, with geometry factors differing by a factor of ~ 100. This way, one of the sections will have counting rates which are statistically meaningful and which at the same time can be handled by the time-of-flight electronics. However, intense ion fluxes can in some cases saturate the CODIF instrument (particularly if data are acquired from the high sensitivity side), but these fluxes are measured with HIA. The operation of the high-sensitivity side ("high-G", or "HS") and of the low-sensitivity side ("low-g", or "LS") on CODIF is mutually exclusive, and only one of the two sides can be selected at a time to supply data.

With an additional Retarding Potential Analyser (RPA) device in the aperture system of the CODIF sensor, and with pre-acceleration for the energies below 25 eV/e, the range is extended to energies as low as the spacecraft potential. The retarding potential analyser operates only in the RPA mode, and provides an energy range between about 0.7 and 25 eV/e (with respect to the spacecraft potential).

2.2 The HIA (CIS-2) Instrument

The HIA instrument is an ion energy-spectrometer, capable of obtaining full three-dimensional ion distributions with good angular and time resolution (one spacecraft spin). HIA combines the selection

of incoming ions, according to the ion energy per charge by electrostatic deflection in a quadrispherical analyser, with a fast imaging particle detection system. This particle imaging is based on microchannel plate (MCP) electron multipliers and position encoding discrete anodes. As for CODIF, ions are selected as a function of their E/q (energy per charge) ratio, by sweeping the high voltage applied between the two hemispheres, cf. Fig. 2.2.

In order to cover populations ranging from solar wind and magnetosheath ions to tail lobe ions, a dynamic range of more than 10^5 is required. HIA therefore consists of two 180° field-of-view sections, with two different sensitivities (with a ~20 ratio), corresponding respectively to the high-sensitivity ("high-G", or "HS") and to the low-sensitivity ("low-g", or "LS") side. The "low g" side allows detection of the solar wind and the required high angular resolution is achieved through the use of 8 sectors (or MCP anodes), 5.625° each, the remaining 8 sectors having 11.25° resolution. The 180° "high G" side is divided into 16 sectors, 11.25° each. For each sensitivity side a full 4π steradian scan, consisting of 32 energy sweeps, is completed every spin of the spacecraft, i.e. every 4 s, giving a full three-dimensional distribution of ions in the energy range ~5 eV/e - 32 keV/e.

3 Measurement Calibration Procedures

3.1 Calibration files

Both CODIF and HIA have been very well calibrated before launch, in vacuum test facilities (Rème et al., 2001). However, due to the in-flight evolution of the MCP detection efficiencies as a function of time, the CIS calibration files are updated regularly. A calibrations catalogue file, which is provided with the calibration files, serves as a pointer to which calibration files to use for each data time period. This catalogue file evolves in an incremental way through the mission, to take into account the existence of new calibration files, which correspond to the instrument particle detection efficiency evolution, or other changes in the instrument.

Calibration files include thus:

- parameters that have been determined during ground calibrations in vacuum test facilities and are stable through the mission (e.g. instrument angle response, electrostatic analyser constant used in the calculation of the energy sweep tables, etc.),
- parameters that change gradually through the mission (e.g. particle detection efficiencies),

- parameters that can be changed during the mission by command (e.g. upload of new spin accumulation tables for 3-D ion distributions in the various modes).

All of them are equally important in converting raw data into physical units, and are used together. How the calibration values are used to convert particle raw counts in physical units, such as particle flux, or moments of the ion distribution functions, is described in the Appendix of the CAA-CIS Interface Control Document (Dandouras and Barthe, 2013).

3.2 Detector efficiency

Detection efficiency degrades with time, due to the MCP gain fatigue mechanism (Prince and Cross, 1971). The physical degradation of the MCPs during the mission is in some extent compensated by applying increased high voltages on the MCP plates, to restore as much as possible secondary electron gain in the MCP channels albeit the physical degradation of their emissive surfaces. The procedure used onboard for testing the necessity for an eventual MCP HV increase in shown in Figure 3.1.

Updating the calibration files for the detection efficiency evolution, with respect to the pre-launch calibrations, is a multi-step process, and is performed a few times per year, or any time when the MCP voltage is changed.

3.2.1 Determination of HIA efficiency

For HIA the **detection efficiency** is given by:

$$\boldsymbol{Eff}\ (PF, E)^{-1} = Norm\_\Theta * Eff(E) * Cheff(\Theta) * [\,1 / T(E)]$$

where:

- E is the ion energy
- $Norm\_\Theta$ is an anode normalisation coefficient (one value for the HS and one for the LS side)
- $Eff(E)$ is an Energy-dependent efficiency term, given by $Eff(E) = A * E + B$ (A, B : linear coefficients, one for the HS and one for the LS side)
- $Cheff(\Theta)$ is an Anode - dependent efficiency coefficient
- $T(E)$ is an MCP energy-dependent efficiency, given by $T(E) = T_0 + T_1*(E+E_g) + T_2*(E+E_g)^2$ (E_g : MCP grid acceleration energy)

This results in 41 efficiency calibration coefficients per validity period per spacecraft (2 + 4 + 32 +3). These coefficients need to be determined for each validity period that is determined by the MCP aging and/or MCP voltage variations.

In addition, g_E is an energy-independent geometric factor (one for the HS side and one for the LS side.

During the in-flight calibration procedure the HIA ion density values are compared and cross-calibrated with the electron density values supplied by the Whisper sounder experiment (Décréau et al., 2001). This is performed in the magnetosheath for the HS side and in the solar wind for the LS side, i.e. in the plasma environment where each of the two sides has the optimum performance, and where the plasma energy spectrum is within the energy domain covered by the instrument. It should be noted also that the HIA anodes relative efficiencies are remarkably stable, i.e. the efficiency drift is very homogeneous between the anodes (11.25° or 5.625° sectors).

More details for the HIA in-flight calibration procedure are given in Blagau et al., 2014.

3.2.2 Determination of CODIF efficiency

For CODIF, and for each of the four main ion species detected (H^+, He^{++}, He^+, O^+), the **detection efficiency** is given by:

$$\boldsymbol{Eff}\,(PF, E, m) = (M_0 + M_1*E + M_2*E^2 + M_3*E^3\ )\ *\ Abs\_Eff$$

where:

- M_0 ... M_3 are the efficiency calibration coefficients, depending on the ion species m (4 sets, for H^+, He^{++}, He^+, and O^+), and on the detection anode PF
- E is the total ion energy (ion energy + post-acceleration energy)
- Abs_Eff is the absolute efficiency (one value per ion species m for the HS and one for the LS side)

This results in 232 efficiency calibration coefficients per spacecraft (4 x 4 x 14) + (2 x 4). These coefficients need to be determined for each validity period that is determined by the MCP aging and/or MCP voltage variations.

In addition, g_E is an e energy-independent geometric factor (one for the HS side, one for the LS side and one for the RPA).

The CODIF calibrations updating is a more complex process. It involves the determination of the start-MCP efficiency, the stop-MCP efficiency, the fraction of coincidences between the “start” time-of-flight signal and the “stop” time-of-flight signal that also have a “single position” signal, allowing thus to calculate the total efficiency. In addition, the efficiencies of the individual anodes (22.5° sectors) have to be cross-calibrated, since they slowly drift relative to each other, and this is performed by using

time periods when the ion distributions are expected to be gyrotropic. CODIF calibrations involve also separate efficiencies determination for H^+ and O^+ ions.

Plasma pressure balance control, at the transition of plasma boundaries, is an additional tool for calibrating the CODIF efficiencies (Fig. 3.2).

The resulting CODIF H^+ measurements are also cross-checked with the HIA measurements, for periods when the plasma is composed mainly from H^+ ions, and with WHISPER, PEACE and WBD density data, when all these instruments are covering well the ambient plasma energy range. CODIF data are also cross-checked with the high-energy ion data supplied by the RAPID experiment (Wilken et al., 2001), for periods where energetic plasma is present in the energy range of both instruments (Kronberg et al., 2010).

The key issues during the CODIF in-flight calibrations are (see Fig. 3.3):

Overall Change in H^+ Efficiency:

- For Cluster spacecraft 4 use "monitor rate" data to track the start efficiency (SFR/SR: start/stop coincidence rate to stop rate), stop efficiency (SFR/SF) and the fraction of coincidences that also have a single position signal (SEV/SFR). The product of these values gives the total efficiency (cf. also Figs. 5.1.1 and 5.1.2).
- For Cluster 3 (for which the Stop rate, SR, does not work well) use comparison spectra with Cluster 4 for time periods when the two spacecraft are close.

Overall Change in O^+ Efficiency:

- We used to use times when the count rate was dominated by O^+ (mainly times with O^+ "beams" in the lobe).
- Because these do not give any more a sufficiently high count rate (since 2007), we instead now use comparison of O^+ spectra between Cluster 3 and Cluster 4, and assume that Cluster 3 is constant.

- Analysis of long-term trends (over a solar cycle) of the O+/H+ ratio has been also performed, in 2013, which allowed a reassessment of the O^+ efficiency values after 2006 (cf. section 5.1.2).

Relative efficiency change between anodes for Cluster 3 and Cluster 4, H^+ and O^+:

- Use pitch angle spectra during gyrotropic time periods to normalise the different positions (anodes) within each instrument. This is done separately for H^+ and O^+.

More details for the CODIF in-flight calibration procedure given in Kistler et al., 2013.

4 Measurement Processing Procedures

The processing of the CODIF and HIA particle raw counts with calibration values, and their conversion into physical units, such as particle flux or moments of the ion distribution functions, is described in the Appendix of the CAA-CIS Interface Control Document (Dandouras and Barthe, 2013).

The data processing requires three elements: CIS raw (L1) data, calibration files and the PI software. The processing is fully automated and produces output data files in CEF format.

5 Results of Calibration Activities

5.1 CODIF

For CODIF the efficiency degradation is pronounced, due to the operational principle of this instrument, requiring the detection of both the ion ("stop" time-of-flight signal) and of the electrons emitted by the carbon foil ("start" time-of-flight signal), plus a "position" signal, to validate the detection of an ion.

In 2008 the efficiencies for CODIF were reduced, on the average, to about 2% of the initial detection efficiencies on Cluster 4, and to less than about 5% on the "good" MCP quadrant on Cluster 3 (cf. CIS data caveats in Dandouras et al., 2010). In spite of these low efficiency values, the CODIF performance and ability to still collect data of quality adequate for addressing most of its scientific objectives is remarkable.

In July 2009 the CODIF MCP high-voltage on Cluster spacecraft 4 was raised by ~80 V, which increased the particle detection efficiency by a factor of ~2 and brought the efficiency back to the summer 2005 levels. Since then, the CODIF detection efficiency has been remarkably stable. However, a slow efficiency decline tendency appeared again in 2015-2016.

The key limitations are:

- **Cluster 1**: The CODIF instrument is switched off since 25 October 2004, due to an MCP high voltage anomaly.
- **Cluster 3.** The CIS instrument (CODIF and HIA) is switched off since December 2009, due to a damaged electronic component in the instrument. In addition, before this, on the HS side only the upper quadrant of CODIF had adequate efficiency, resulting in a poor quality of moments.

5.1.1 H^+ efficiencies

CODIF calibration results, and efficiencies evolution for H^+ are given in Figures 5.1 to 5.3.

Figure 5.1.1 shows the evolution of each of the three signals, i.e. "stop" time-of-flight signal, "start" time-of-flight and "position" signal (cf. section 3.2.2) for Cluster 4, from the beginning of the mission until late 2012. A "zoom" for the period starting from September 2006, with an extension up to July 2015, is provided in Figure 5.1.2.

Figure 5.2 shows the total efficiency evolution for this spacecraft, separately for the HS and the LS. The efficiency improvement, resulting from the MCP high-voltage increase in July 2009, is clear in Figures 5.1 and 5.2. Since then, efficiency changes in this instrument are small.

The total H^+ efficiency evolution, for the three Cluster spacecraft, is shown in Figure 5.3.

5.1.2 O^+ efficiencies

Figure 5.4 shows the evolution of MCP efficiencies for O^+ on Cluster 1 and 4. Note that, for Cluster 4, the O^+ efficiency was revised in 2013, following the analysis of long-term trends (over a solar cycle) of the O^+/H^+ ratio. The H^+ efficiency is shown for comparison.

5.1.3 Inter-anode comparisons

Figure 5.5 shows the comparison of inter-anode efficiencies for H^+ on Cluster 3 and Cluster 4. As discussed in section 3.2.2, pitch-angle distribution plots are used in areas where the plasma distribution is expected to be gyrotropic in order to adjust the inter-anode efficiencies.

5.2 HIA

The particle detection efficiency degradation is moderate for the HIA instrument. The physical degradation of the MCPs is in some extent compensated by applying increased high voltages on the MCP plates, to restore secondary electron gain in the MCP channels albeit the physical degradation of

their emissive surfaces. These high voltage increases are shown in Figure 5.6. Since February 2007 there has been no other change in these MCP high voltages.

5.2.1 Inter-anode comparisons

The HIA relative anode response, in an isotropic plasma, is shown in Figure 5.7.

It should be noted also that the HIA anodes relative efficiencies are remarkably stable, i.e. the efficiency drift is very homogeneous between the anodes (11.25° or 5.625° sectors).

5.2.2 Variation of HIA efficiency

Figure 5.8 gives the evolution of the HIA HS and LS calibration factors for Cluster 1 (black) and Cluster 3 (red), following the high voltage increases on the MCP plates. Data here are plotted from the beginning of the mission until October 2015. For comparison with CODIF cf. Figures 5.1 to 5.4.

Note that the Cluster 1 HS is the only operational side of the instrument since 2012.

6 Results of Cross-Calibration Activities

As indicated in section 3, the HIA ion density values are compared and cross-calibrated with the electron density values supplied by the Whisper sounder experiment (Décréau et al., 2001). This is performed in the magnetosheath for the HS side and in the solar wind for the LS side, i.e. in the plasma environment where each of the two sides has the optimum performance, the plasma energy spectrum is within the energy domain covered by the instrument and spacecraft charging effects are negligible.

6.1 HIA efficiency

Figure 6.1 shows a typical example of HIA - Whisper density cross-calibration in the magnetosheath (HS side). It is from a May 2009 event, used in fine-tuning HIA calibrations. 2777 data points were used in this example, and the root-mean-square deviation of the HIA to Whisper calculated densities is here 3.7 %. Similar procedure is used in the solar wind, to fine-tune the LS side of HIA.

Figures 6.2 shows an example of density comparison between the HIA instrument and the Whisper experiment, in the magnetosheath (Cluster 1 and Cluster 3). The fit between the two density plots is excellent.

6.2 CODIF efficiency

Figure 6.3 shows the same example for CODIF onboard Cluster spacecraft 4, where the LS side is operating, which is the one suited for the magnetosheath. Notice that on spacecraft 4 the CODIF LS side is used in the magnetosheath, in order to have better ion moments, as HIA is off on this spacecraft. Again the fit between the two density plots can be very good.

However, there are cases where the two instruments do not give the same results. Section 6.2 of the CIS Users Guide (Dandouras and Barthe, 2017) discusses the conditions where such discrepancies can appear, and the related caveats. Section 6.1 of the CIS Users Guide provides a data selection guide, in order to help the user select the most appropriate of the two instruments, as a function of the plasma environment analysed.

Figure 6.4 shows a typical example for HIA and CODIF density values comparison with the WHISPER provided density in the cusp, where the spacecraft is going through a large dynamic range of density values. The negative of the spacecraft potential value, measured by the EFW experiment, is also given. In the relatively high-density plasma (> 2 cm^{-3}), where spacecraft charging effects are small, the fit between the two CIS instruments and the Whisper density measurements is very good. In the low density part,

however, where spacecraft charging to a positive floating potential repels the low-energy ions, which cannot any more be detected by CIS, HIA and CODIF provide, as expected, underestimated density values.

Figure 6.5 shows a case of CODIF density values comparison with the PEACE provided density in the magnetotail plasma sheet. This is a case of a dense plasma sheet (> 1 cm^{-3}), where spacecraft charging is low, and the two experiments give very consistent density values. This is not however the case in more typical tenuous plasma sheet events (< 1 cm^{-3}), where spacecraft charging to a positive floating potential does not allow the detection by CIS of low-energy ions.

The CODIF ion flux values have been also controlled for consistency with the RAPID-IMS flux values, in the overlapping energy range of the two instruments (~29-40 keV/e). Since the energy bins of the two instruments do not exactly match each other, this involved a comparison by fitting kappa distribution functions through the energy spectra of the two instruments (Kronberg et al., 2010). Figure 6.6 provides an example of such a cross-calibrated ion energy spectrum in the plasma sheet.

6.3 HIA-CODIF Cross-Calibration

Figure 6.7 shows a comparison of orbit averages of the density and the three components of the velocity for CODIF on Cluster 4, and HIA on Cluster 1 and Cluster 3, in GSE coordinates. The *x* and *y* coordinates are approximately in the spin plane, and so the relative anode efficiency does not significantly affect these velocities. The *z* coordinate is almost along the spin axis, so any discrepancies in the relative anode efficiencies would be observed here. It is expected that the average velocity in *z* should be 0. The relative anode efficiencies are adjusted to keep the error to less than 15 km s^{-1} (Kistler et al., 2013).

7 Summary

In summary, the HIA detection efficiency degradation has been moderate for HIA, more pronounced (but reasonable) for CODIF, due to the operational principle of this instrument.

8 References

Blagau, A., I. Dandouras, A. Barthe, S. Brunato, G. Facskó, V. Constantinescu: In-flight calibration of Hot Ion Analyser onboard Cluster, Geosci. Instrum. Method, 3, 49, doi:10.5194/gi-3-49-2014 (2014)

Dandouras, I., A. Barthe: Cluster Active Archive: Interface Control Document for CIS. CAA-CIS-ICD-0001 (2013)

Dandouras, I., A. Barthe: User Guide to the CIS measurements in the Cluster Active Archive (CAA). CAA-EST-UG-CIS (2017)

Dandouras, I., A. Barthe, E. Penou, S. Brunato, H. Rème, L.M. Kistler, M.B. Bavassano-Cattaneo, A. Blagau, and the CIS Team: Cluster Ion Spectrometry (CIS) Data in the Cluster Active Archive (CAA). In: Proceedings of the Cluster Workshop and CAA School, Springer, p. 51-72,(2010)

Décréau ,P.M.E., P. Fergeau, V. Krasnoselskikh, E. Le Guirriec, M. Lévêque, Ph. Martin, O. Randriamboarison, J.L. Rauch, F.X. Sené, H.C. Séran, J.G. Trotignon, P. Canu, N. Cornilleau, H. de Féraudy, H. Alleyne, K. Yearby, P.B. Mögensen, G. Gustafsson, M. André, D.C. Gurnett, F. Darrouzet, J. Lemaire, C.C. Harvey, P. Travnicek: Early results from the Whisper instrument on Cluster: an overview. Ann. Geophys., **19**, 1241 (2001)

Kistler, L. M., C. G. Mouikis, K. J. Genestreti: In-flight Calibration of the Cluster/CODIF sensor, Geosci. Instrum. Method, 2, 225-235, doi:10.5194/gi-2-225-2013 (2013)

Kronberg, E., P. Daly, I., Dandouras, S. Haaland: Generation and validation of ion energy spectra based on Cluster RAPID and CIS measurements. In: Proceeding of the Cluster Workshop and CAA School, Springer, p. 301-306 (2010)

Masson, A., et al.: Electron density estimation in the magnetotail: a multi-instrument approach. In: Proceedings of the Cluster Workshop and CAA School, Springer, (2010)

Perry, C., T. Eriksson, P. Escoubet, S. Esson, H. Laakso, S. McCaffrey, T. Sanderson, H. Bowen, A.Allen, C. Harvey: The ESA Cluster Active Archive. In: Proceeding of the Cluster and Double Star Symposium-5th Anniversary of Cluster in Space, ESA SP-598, Noordwjik (2006)

Prince, R.H., J.A. Cross: Gain Fatigue Mechanism in Channel Electron Multipliers. Rev. Sci. Instrum., **42**, 66; DOI:10.1063/1.1684879 (1971)

Rème, H., C. Aoustin, J.M. Bosqued, I. Dandouras, B. Lavraud, J.A. Sauvaud, A. Barthe, J. Bouyssou, Th. Camus, O. Coeur-Joly, A. Cros, J. Cuvilo, F. Ducay, Y. Garbarowitz, J.L. Medale, E. Penou, H. Perrier, D. Romefort, J. Rouzaud, C. Vallat, D. Alcaydé, C. Jacquey, C. Mazelle, C. dâUston, E. Möbius, L.M. Kistler, K. Crocker, M. Granoff, C. Mouikis, M. Popecki, M. Vosbury, B. Klecker, D. Hovestadt, H. Kucharek, E. Kuenneth, G. Paschmann, M. Scholer, N. Sckopke, E. Seidenschwang, C.W. Carlson, D.W. Curtis, C. Ingraham, R.P. Lin, J.P. McFadden, G.K. Parks, T. Phan, V. Formisano, E. Amata, M.B. Bavassano-Cattaneo, P. Baldetti, R. Bruno, G. Chionchio, A. Di Lellis, M.F. Marcucci, G. Pallocchia, A. Korth, P.W. Daly, B. Graeve, H. Rosenbauer, V. Vasyliunas, M. McCarthy, M. Wilber, L. Eliasson, R. Lundin, S. Olsen, E.G. Shelley, S. Fuselier, A.G. Ghielmetti, W. Lennartsson, C.P. Escoubet, H. Balsiger, R. Friedel, J-B. Cao, R. A. Kovrazhkin, I. Papamastorakis, R. Pellat, J. Scudder, B. Sonnerup: First multispacecraft ion measurements in and near the Earth's magnetosphere with the identical Cluster ion spectrometry (CIS) experiment. Ann. Geophys., **19**, 1303 (2001)

Wilken, B., P.W. Daly, U. Mall, K. Aarsnes, D.N. Baker, R.D. Belian, J.B. Blake, H. Borg, J. Büchner, M. Carter, J.F. Fennell, R. Friedel, T.A. Fritz, F. Gliem, M. Grande, K. Kecskemety, G. Kettmann, A. Korth, S. Livi, S. McKenna-Lawlor, K. Mursula, B. Nikutowski, C.H. Perry, Z.Y. Pu, J. Roeder, G.D. Reeves, E.T. Sarris, I. Sandahl, F. Søraas, J. Woch, Q.-G. Zong: First results from the RAPID imaging energetic particle spectrometer on board Cluster. Ann. Geophys., **19**, 1355 (2001)

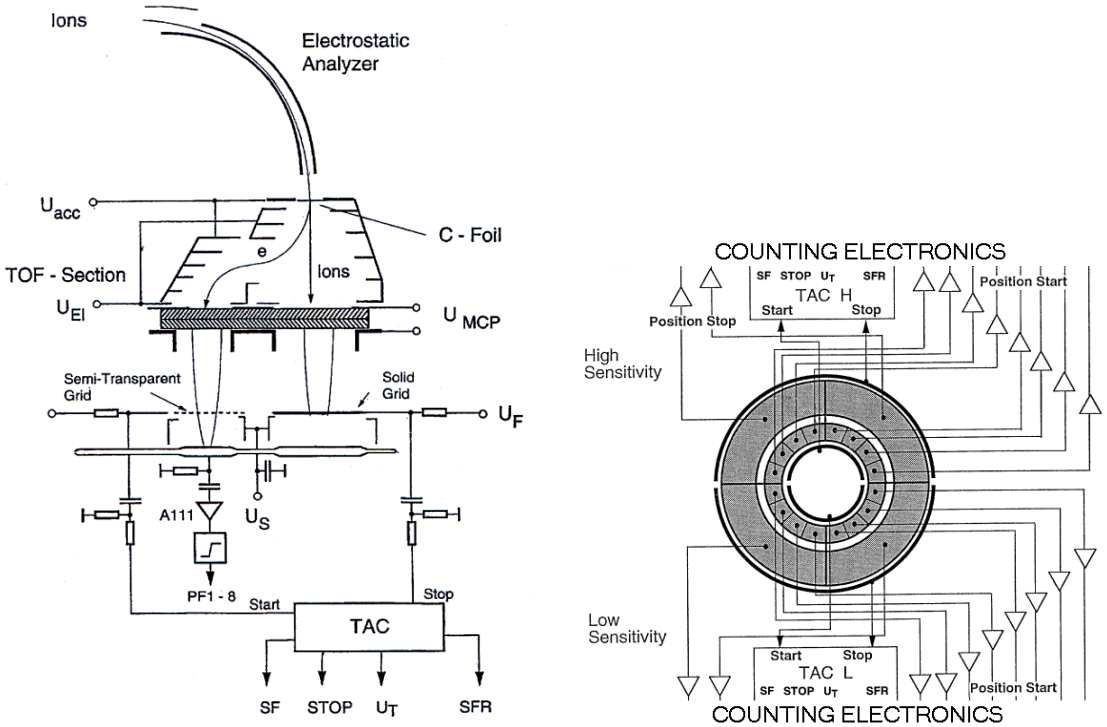

Figure 2.1

Schematic of the CODIF time-of-flight section (left) and MCP sectoring (right).

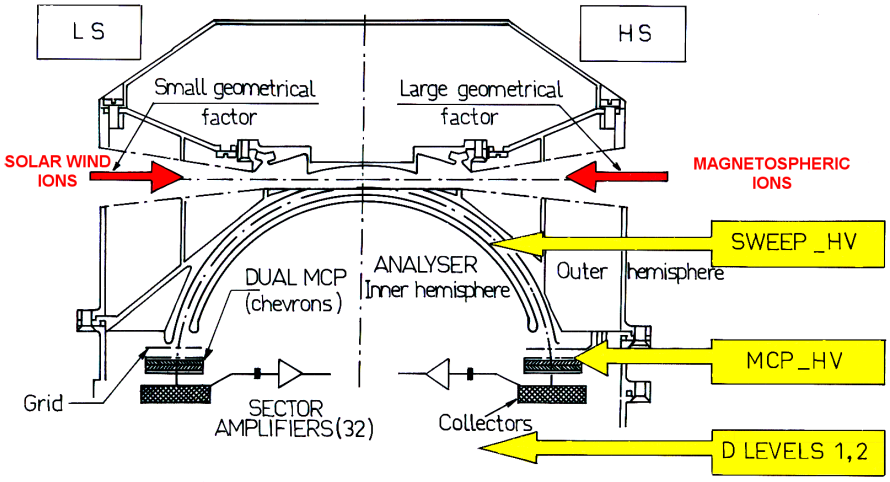

Figure 2.2

Cross sectional view of the HIA instrument.

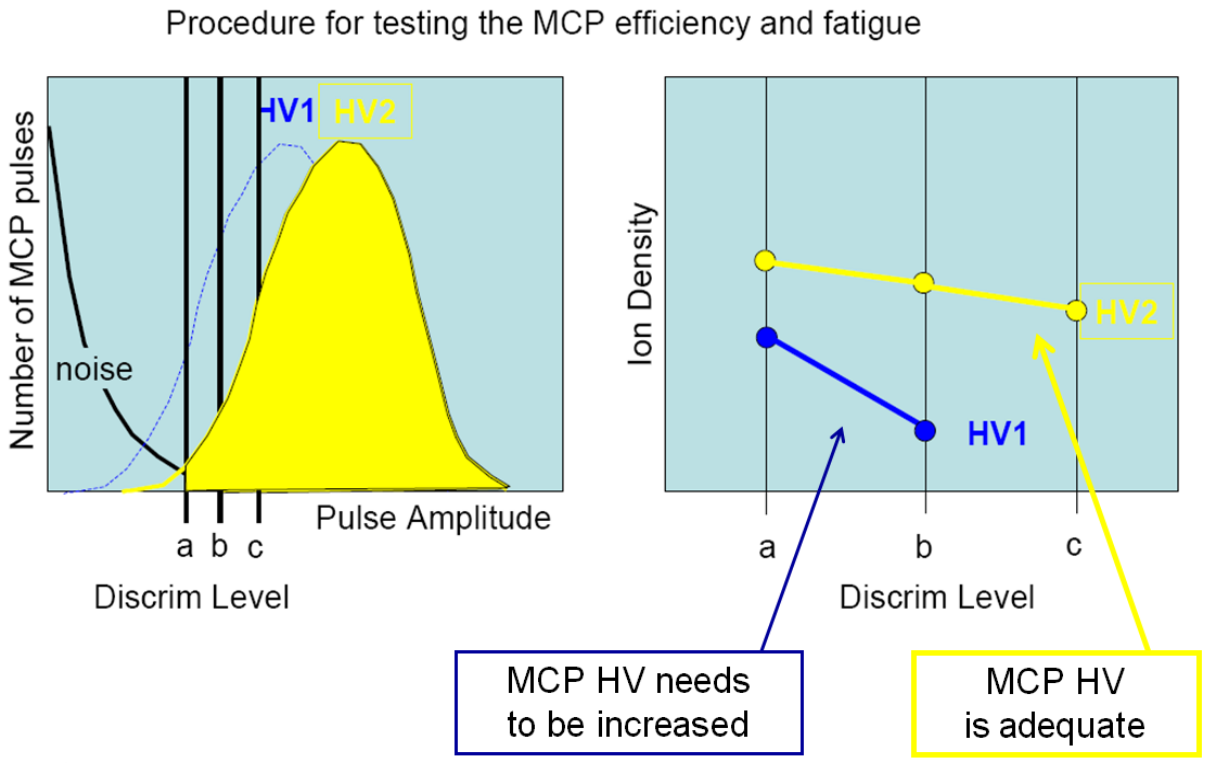

Figure 3.1

Onboard calibration principle:

Procedure for testing the MCP detection efficiency and fatigue.

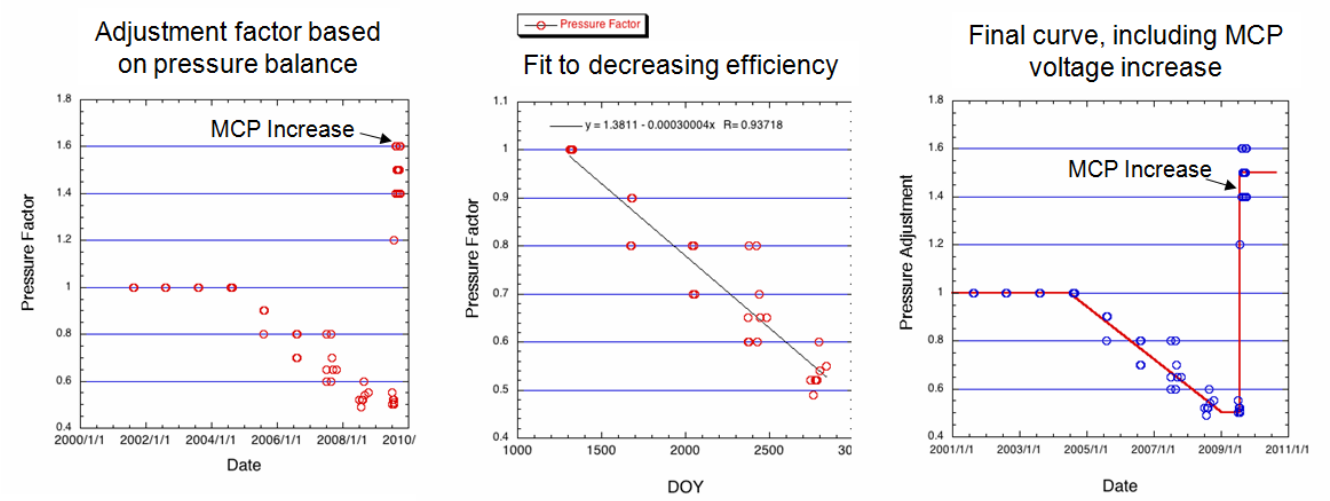

Figure 3.2

Pressure balance test (sum of ion and magnetic field pressure) used for estimating the CODIF efficiency change. It shows the derived pressure balance factor, the fit to the drop-off, and then the final curve. This adjustment is then applied to the current calibration curve.

The CODIF calibrations updating is a complex process. It involves :

- the determination of the start-MCP efficiency
- the stop-MCP efficiency
- the fraction of coincidences between the "start" and the "stop" signal that also have a single position signal, allowing thus to calculate the total efficiency
- In addition, the efficiencies of the individual anodes (for each 22.5° sector) have to be cross-calibrated
- calibrations involve also separate efficiencies determination for the four main ion species

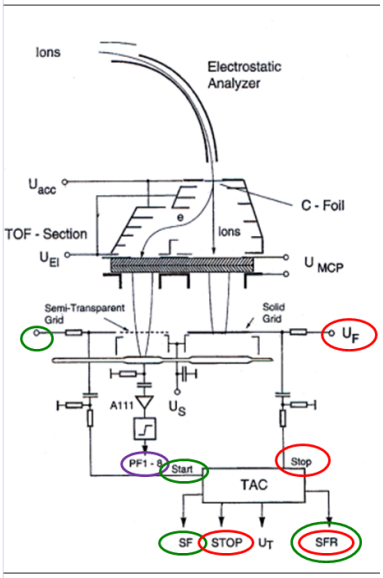

Figure 3.3

CODIF calibrations updating procedure. The main signals, provided by the ion time-of-flight system, are highlighted in the instrument schematic on the right.

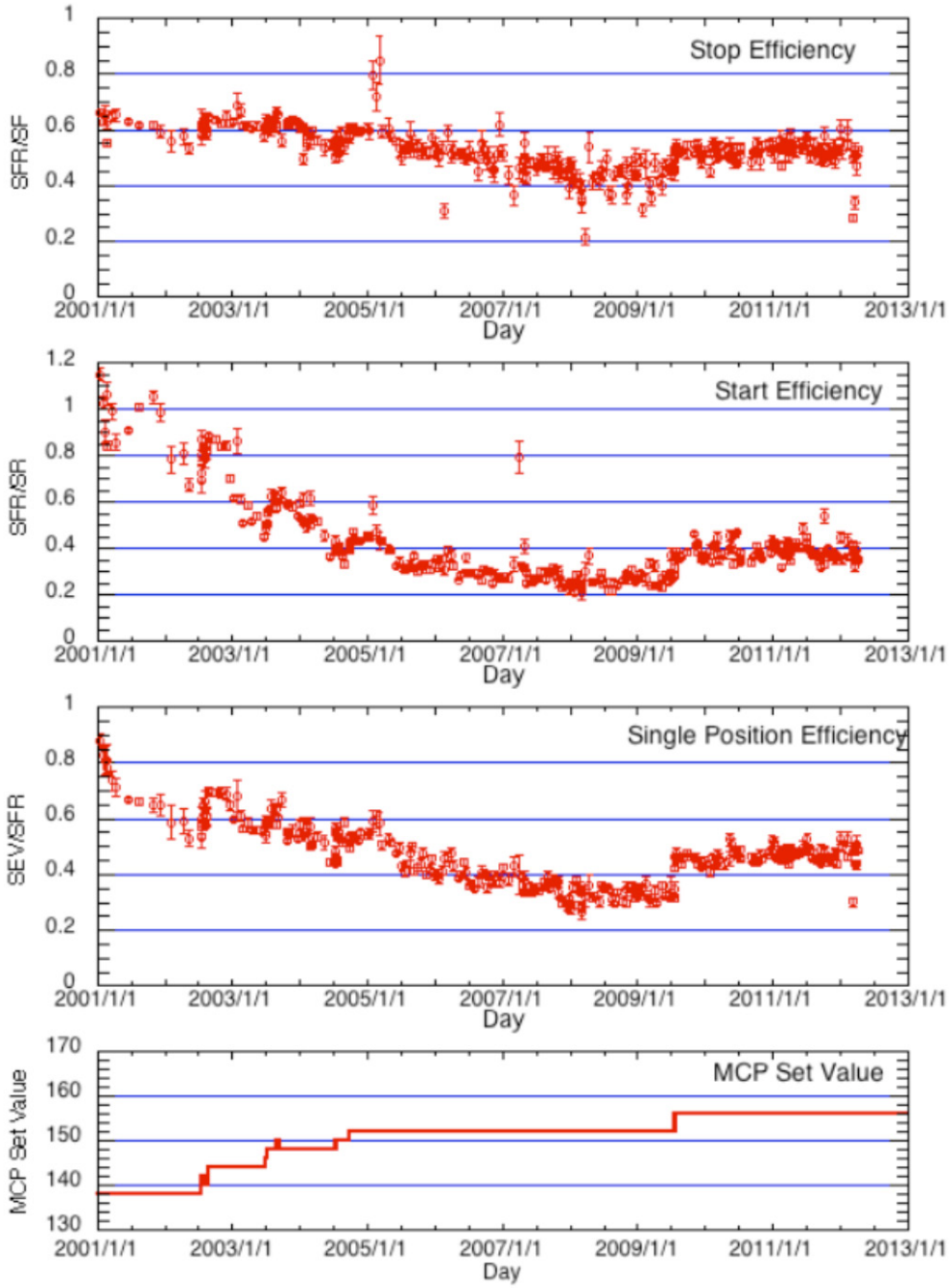

Figure 5.1.1

Cluster 4 CODIF efficiencies for 1 keV H^+ ions, for the "Stop", "Start" and "Single Position" signals. The evolution on the high-voltage value applied on the MCP, through the mission, is in the bottom panel.

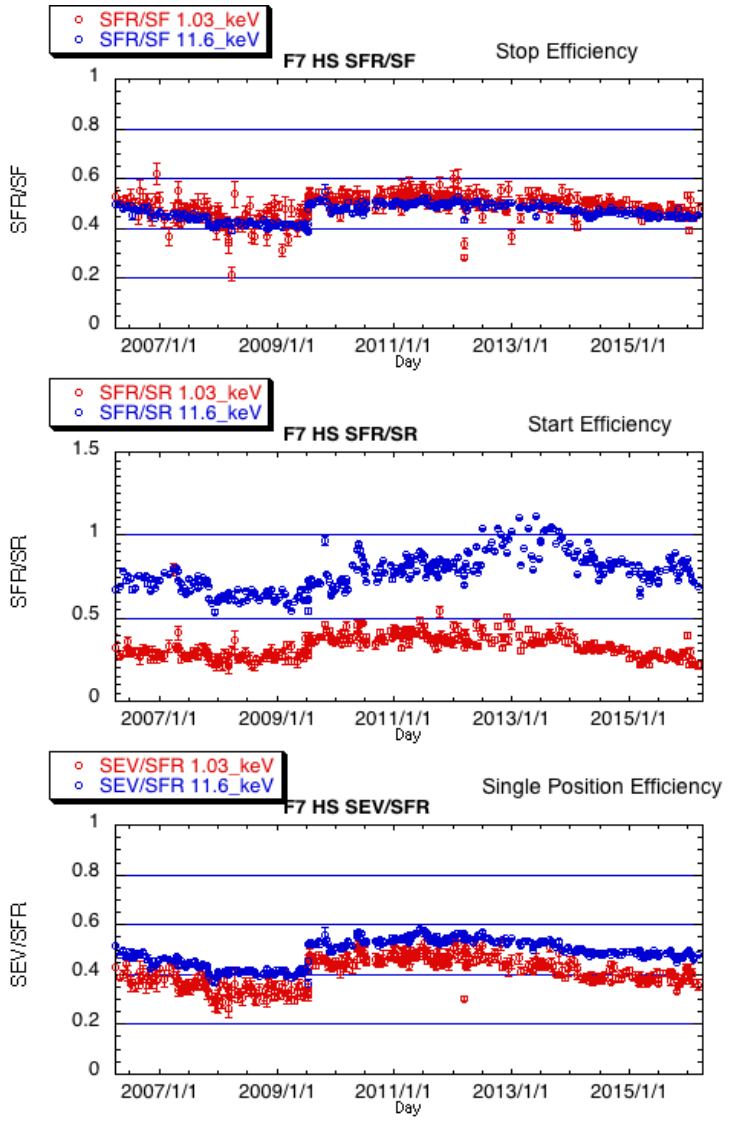

Figure 5.1.2

Cluster 4 CODIF efficiencies for 1.03 keV and for 11.6 keV H^+ ions, for the "Stop", "Start" and "Single Position" signals, for the period September 2006 to July 2015.

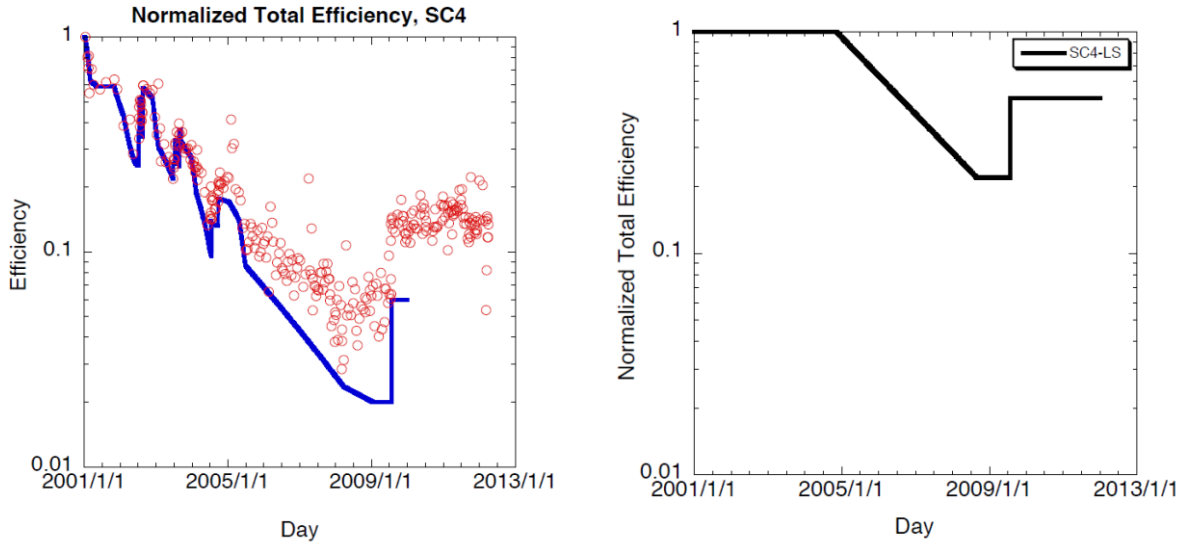

Figure 5.2

CODIF Cluster 4 H^+ efficiency evolution for the HS side (left) and for the LS side (right). Normalized total efficiencies derived using only rate data are shown in red circles, and after the adjustments based on the pressure balance technique are shown with the blue line. All efficiencies are normalized to 1.0 at the start of the mission. From Kistler et al., 2013.

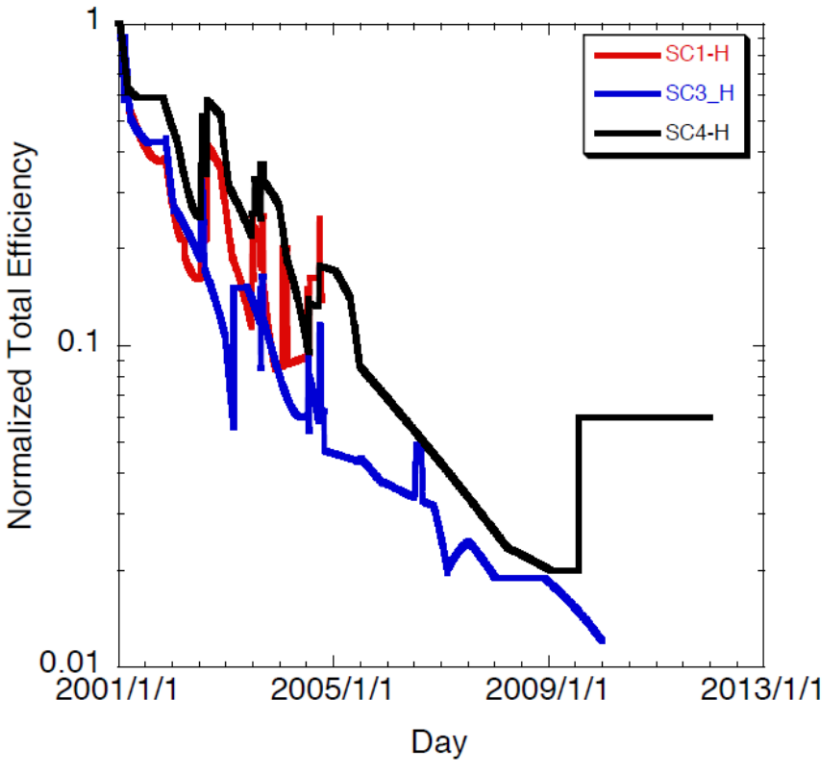

Figure 5.3

CODIF Cluster 1, 3 and 4 total H^+ efficiencies evolution, normalised to the start of the mission. From Kistler et al., 2013.

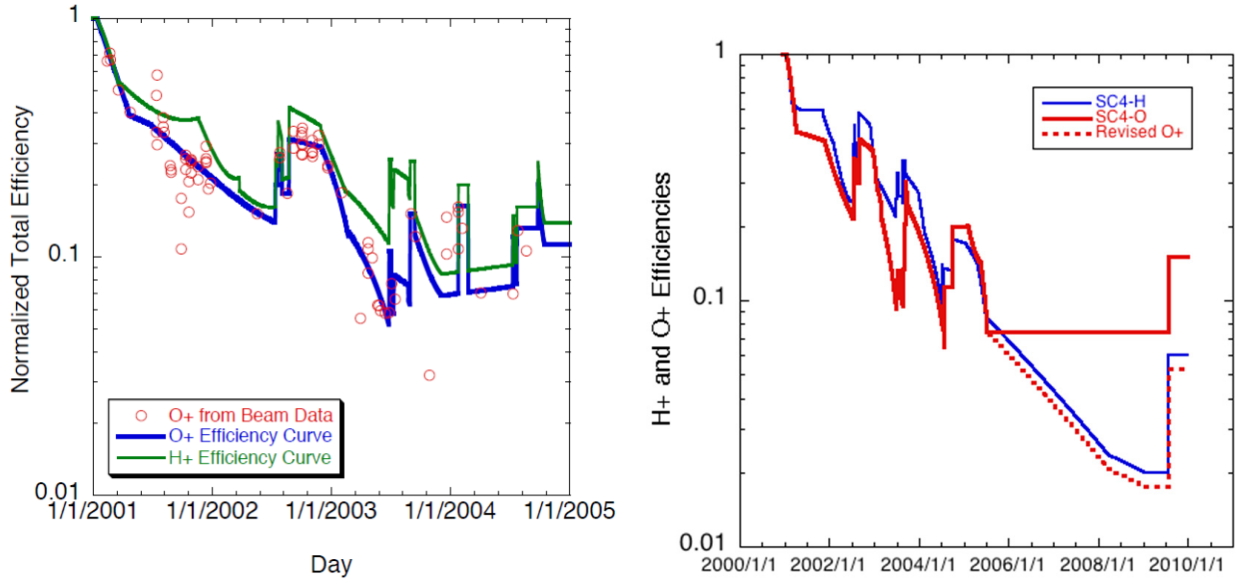

Figure 5.4

CODIF Cluster 1 (left) and Cluster 4 (right) O^+ efficiencies evolution, HS side. Left: O^+ normalized total efficiency derived using the O^+ beam data for Cluster 1. The final curve used for the O^+ efficiency is shown with the blue line, and the H^+ efficiency is shown in green, for comparison. Right: O^+ normalized total efficiency for Cluster 4 (in red). The dotted line shows recently (2013) revised values, obtained from analyzing long-term trends (over a solar cycle) and evolution of the O^+/H^+ ratio. The H^+ efficiency is shown in blue, for comparison.

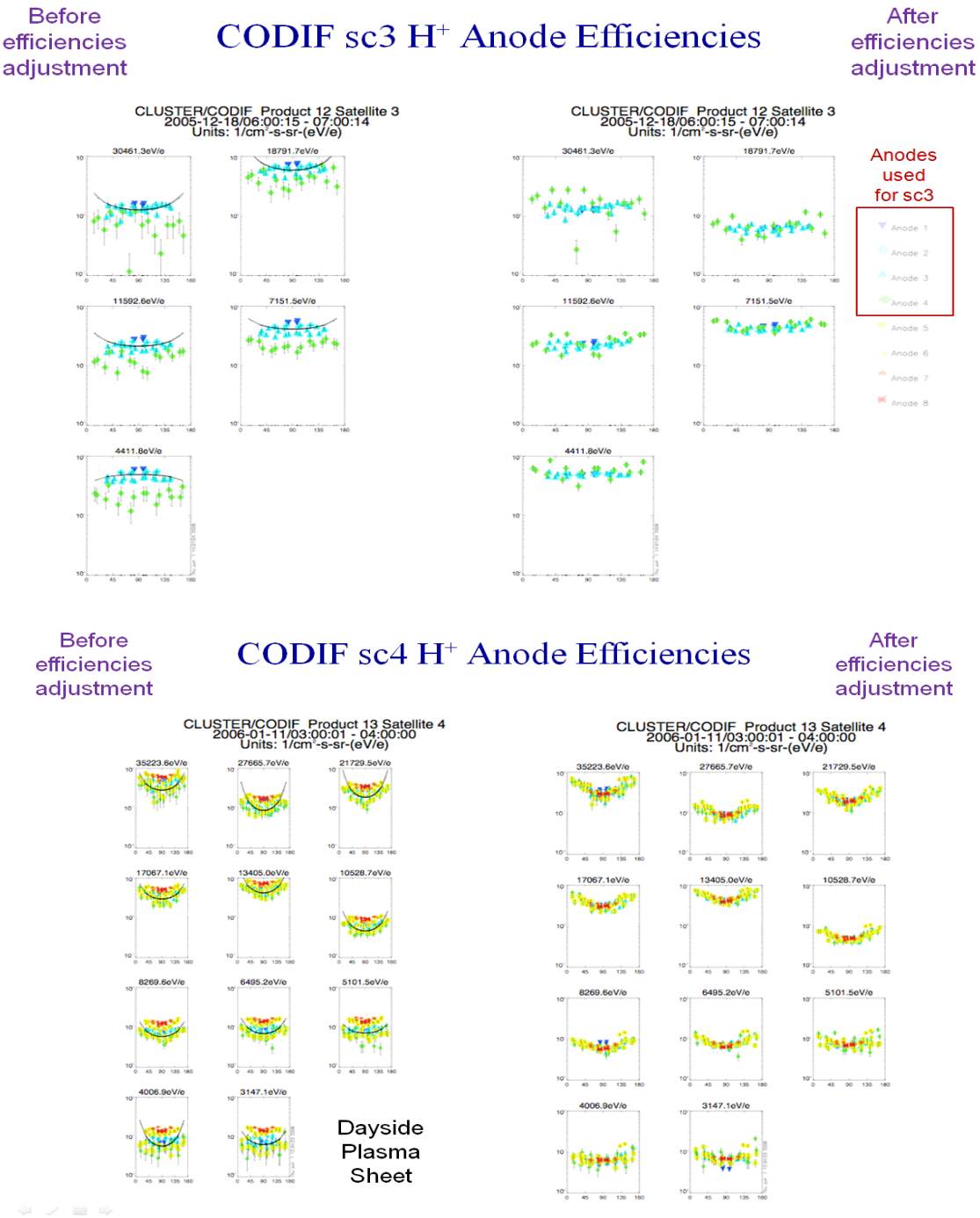

Figure 5.5

CODIF anodes cross-calibrations, in an isotropic plasma: before efficiencies adjustment (left), and after correcting for relative efficiencies (right). Plots are pitch-angle distributions for different energies, and colors correspond to the different anodes.

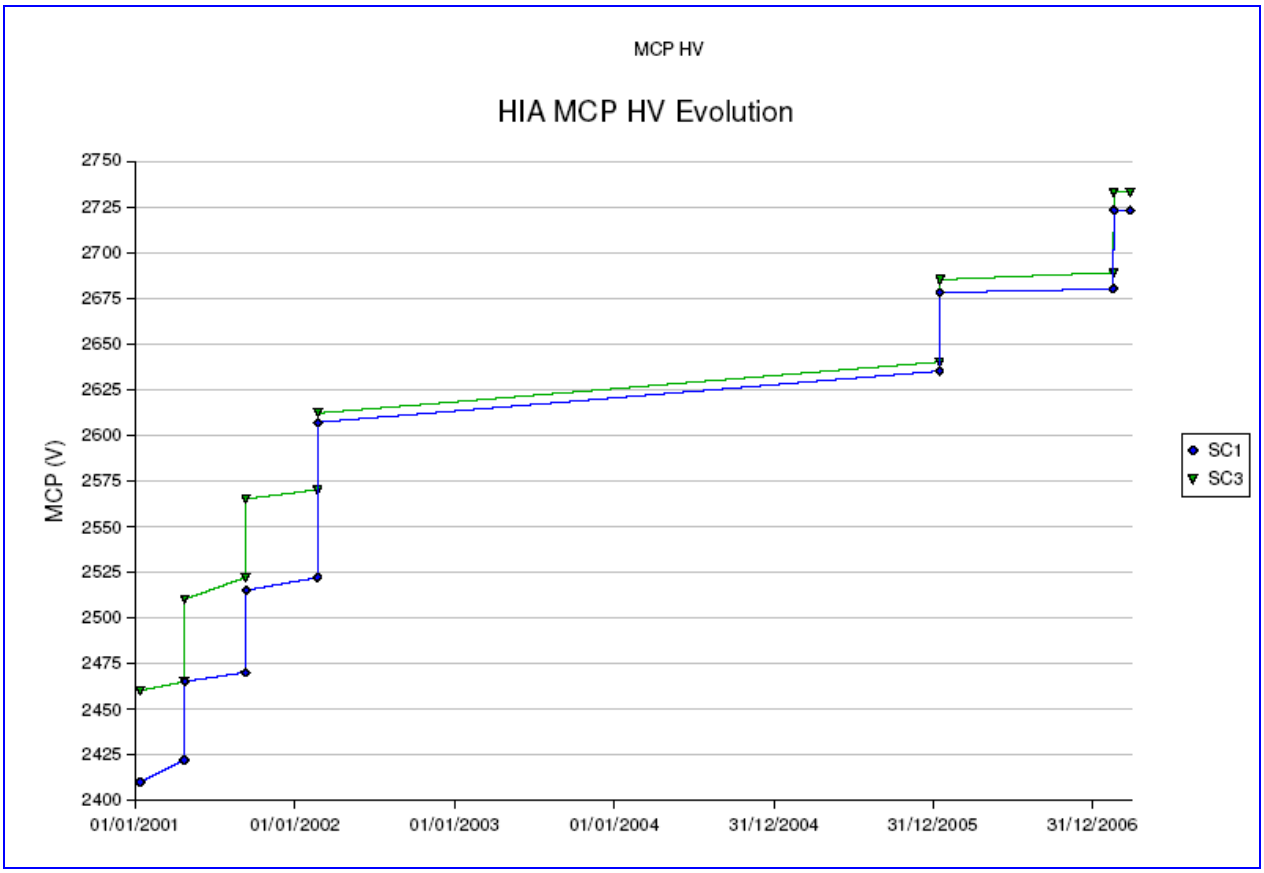

Figure 5.6

HIA MCP HV Evolution.

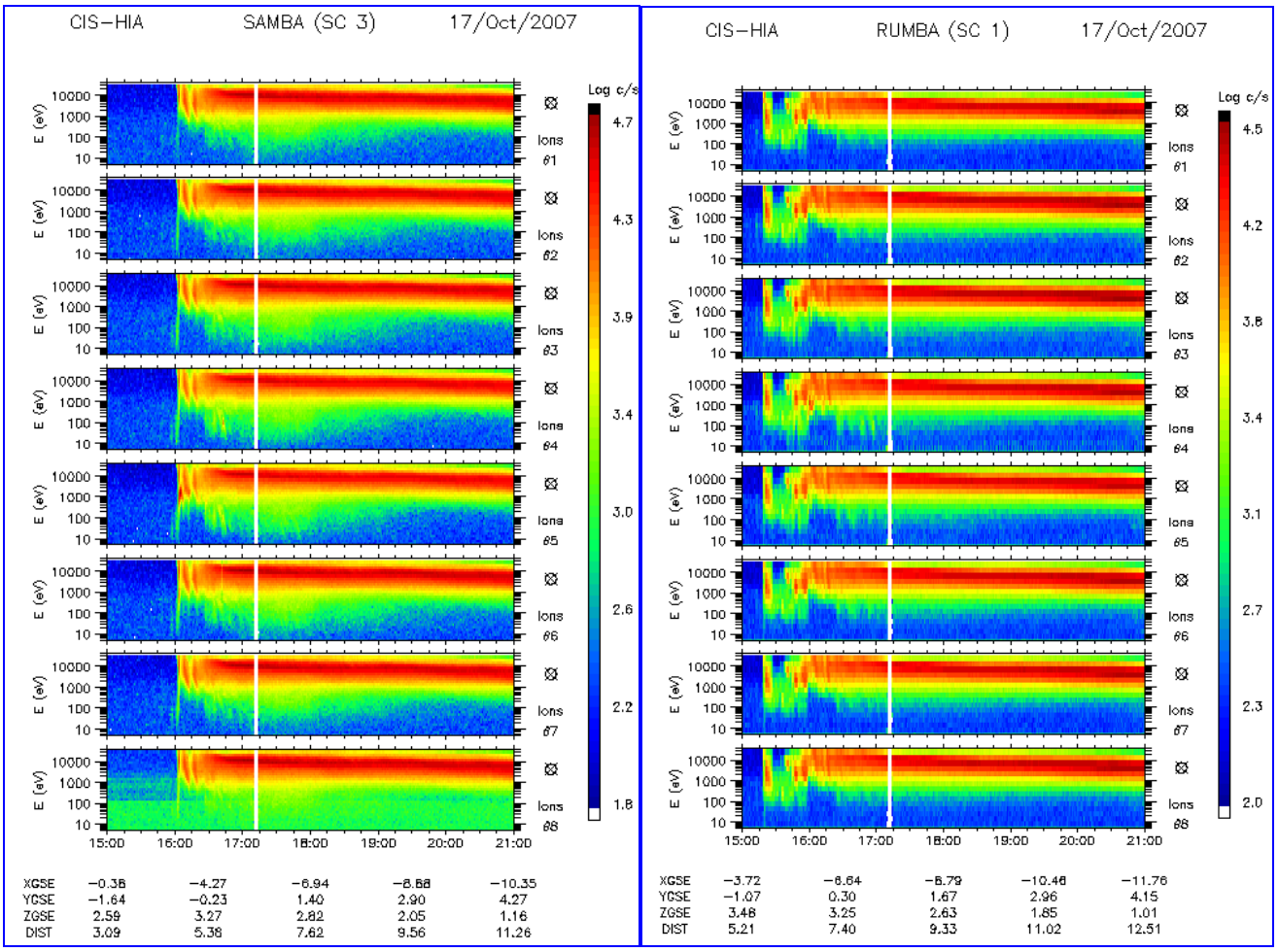

Figure 5.7

HIA MCP anode response in an isotropic plasma (corrected for relative anode efficiencies).

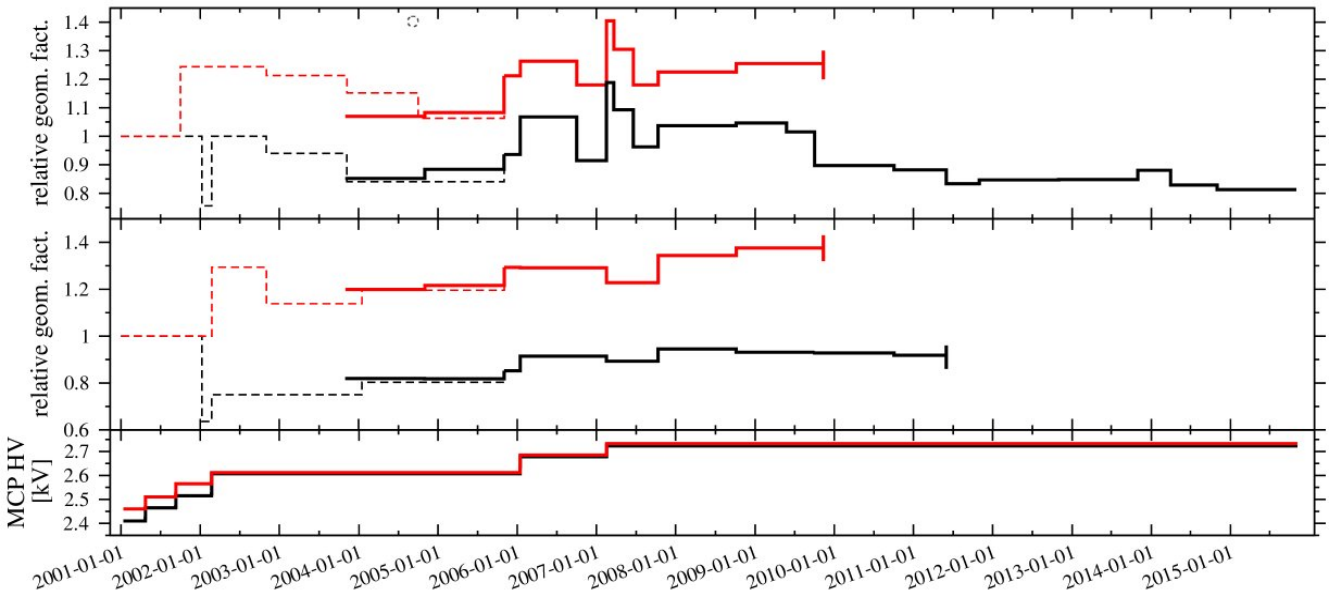

Figure 5.8

Evolution of the HIA calibration factors for Cluster 1 (black) and Cluster 3 (red): HS side (top panel) and LS-side (medium panel). Dashed lines are for in-flight calibrations performed early in the mission. The high-voltage values applied on the MCPs, through the mission, are shown for reference in the bottom panel.

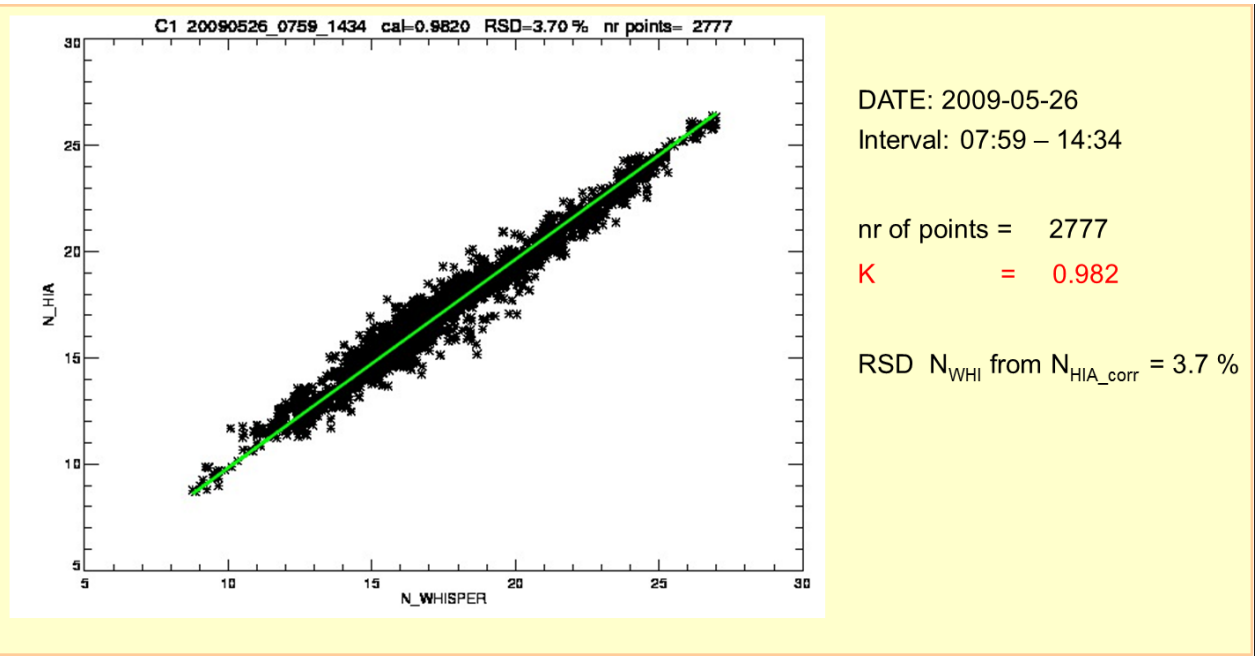

Figure 6.1

HIA - Whisper density cross-calibration in the magnetosheath.

Example of a 2009 event, used in fine-tuning HIA calibrations.

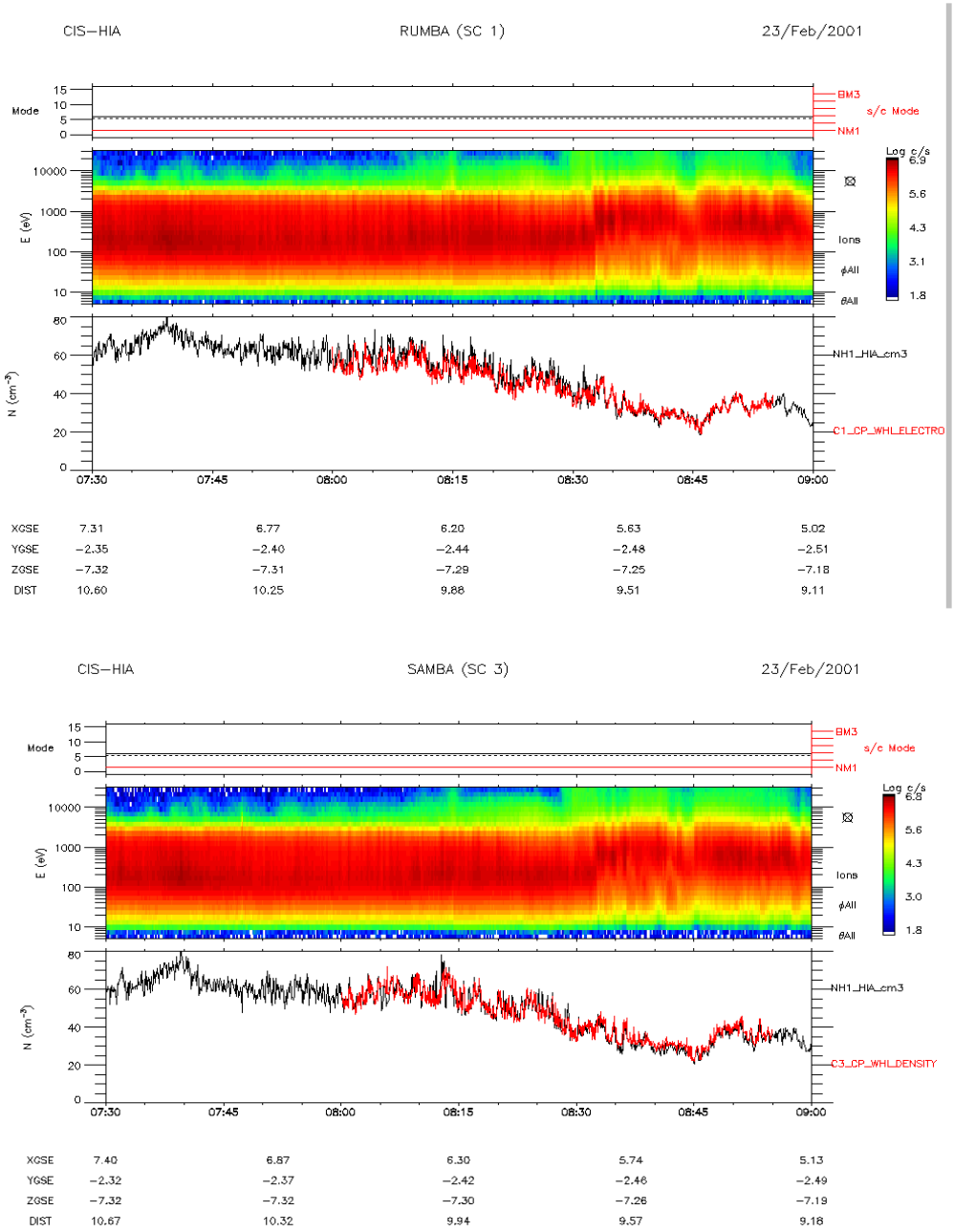

Figure 6.2

Typical HIA - WHISPER density cross-calibration results, in the magnetosheath. HIA density in black, and WHISPER provided density in red. WHISPER density data courtesy of the WHISPER team and the CAA.

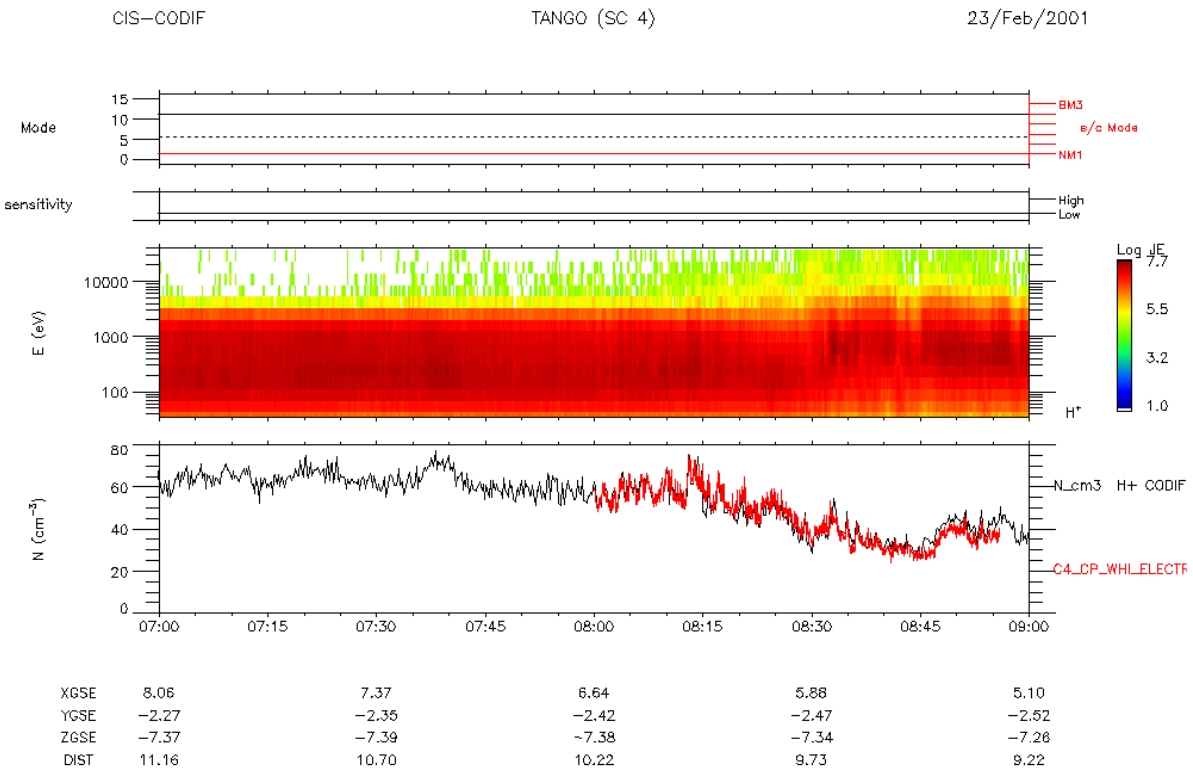

Figure 6.3

Typical CODIF (low-sensitivity side) - WHISPER density cross-calibration results, in the magnetosheath. CODIF density in black, and WHISPER provided density in red. WHISPER density data courtesy of the WHISPER team and the CAA.

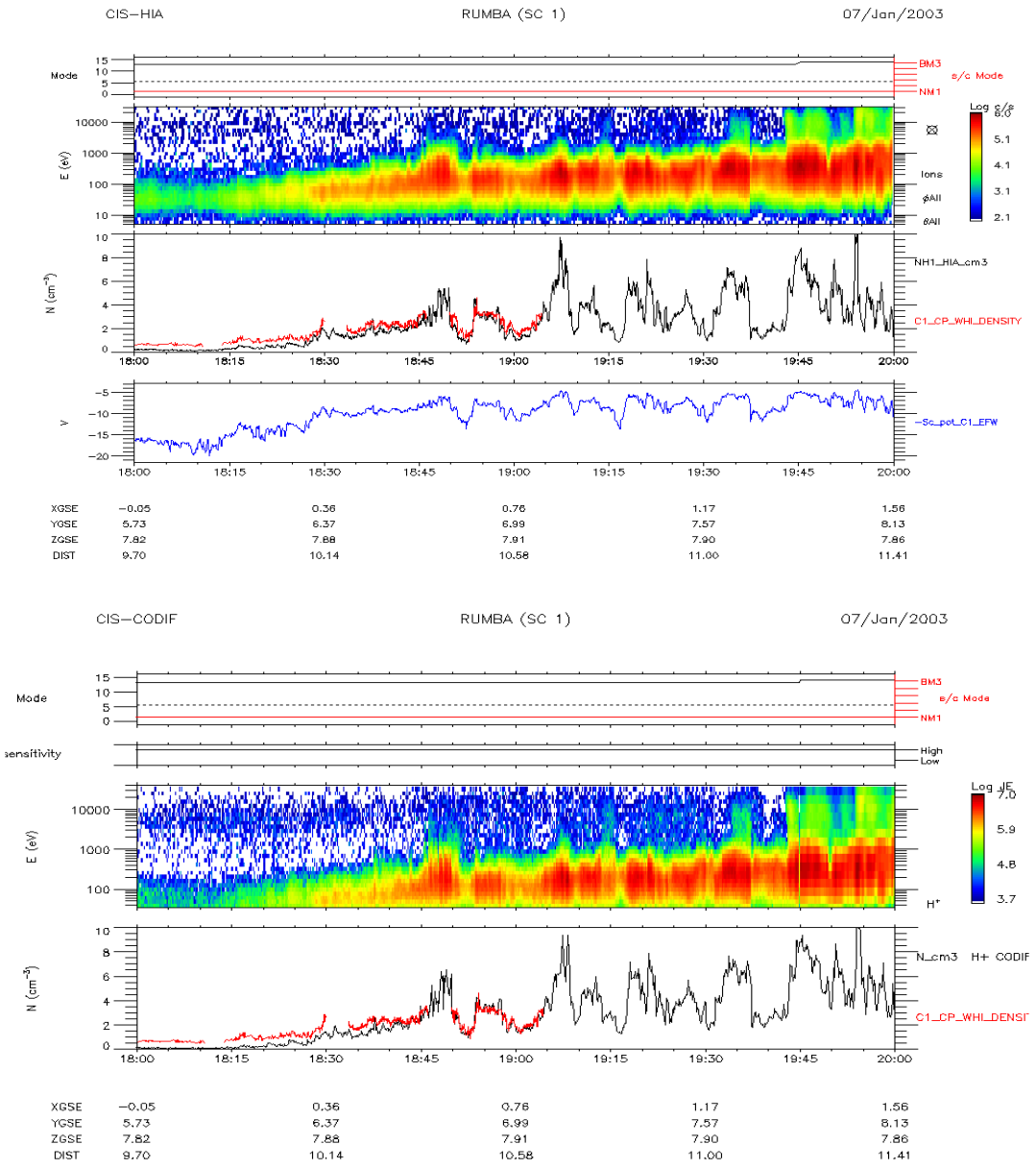

Figure 6.4

Typical HIA (top panels) and CODIF (bottom panels) - WHISPER density cross-calibration results, in the cusp. HIA and CODIF density plots in black (both instruments are operating in the high-sensitivity side), and WHISPER provided density plot in red. In blue is the negative of the spacecraft potential, measured by the EFW experiment. WHISPER data courtesy of the WHISPER team and the CAA. EFW data courtesy of the EFW team and the CAA.

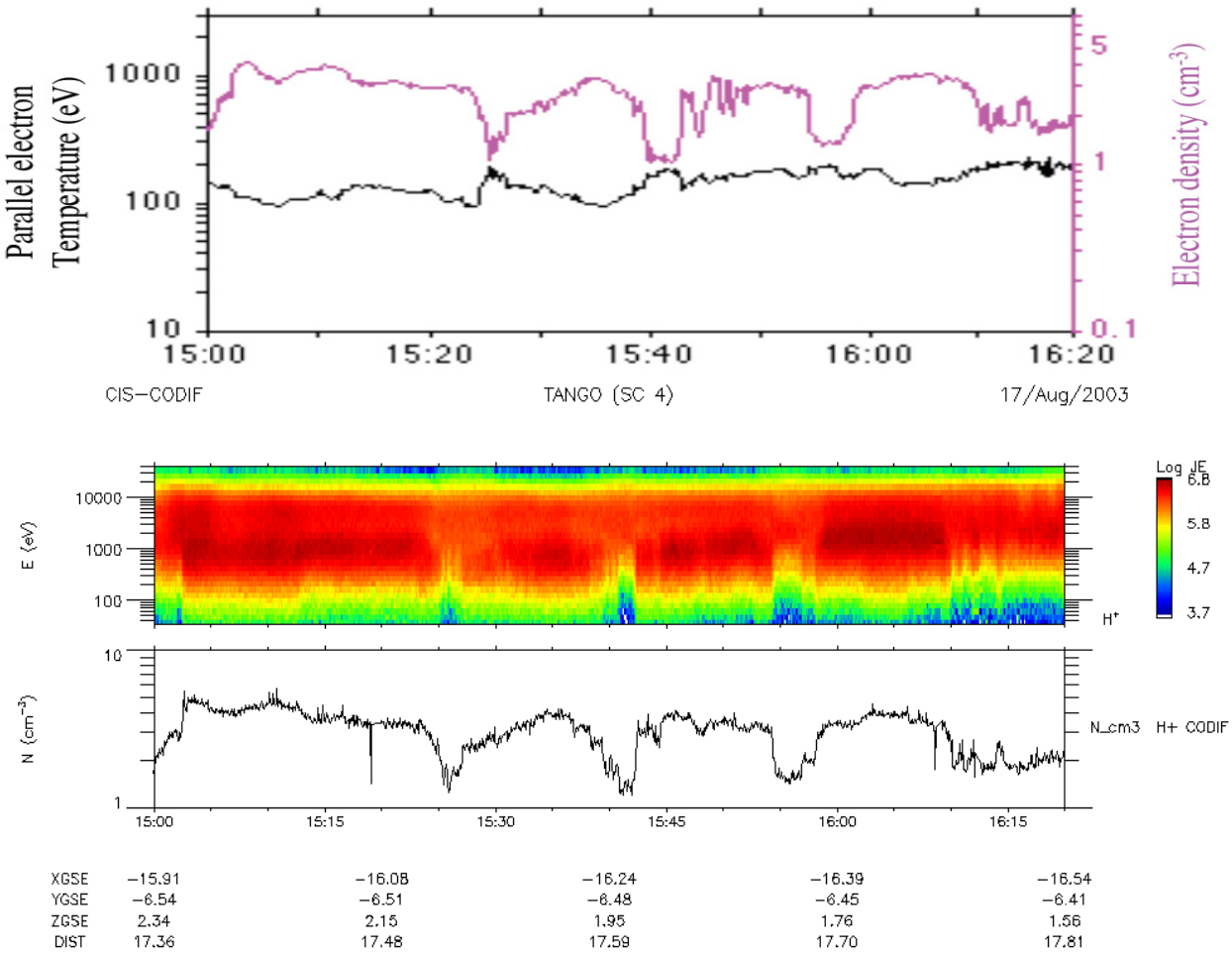

Figure 6.5

PEACE provided density (magenta curve, top panel) compared to CODIF (high-sensitivity side) density (bottom panel) in a dense plasma sheet. From Masson et al., (2010).

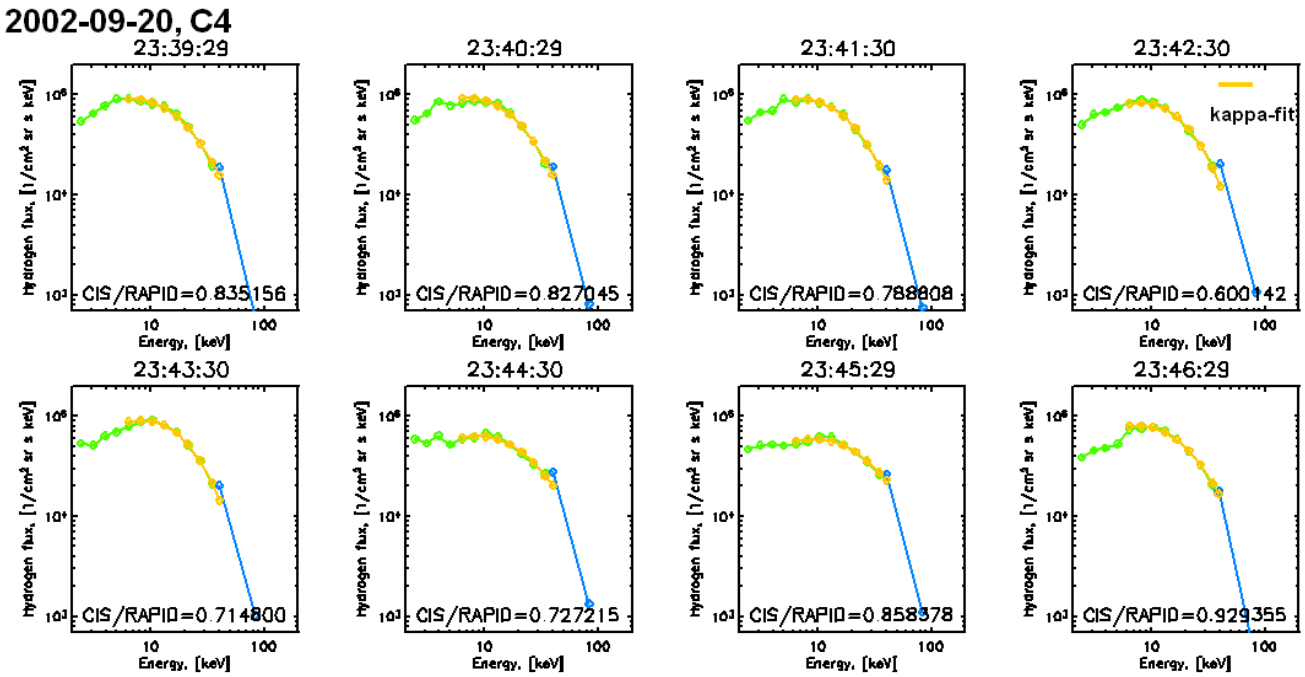

Figure 6.6

Example of composite ion energy spectra: CODIF (green), RAPID (blue), and kappa-fit (yellow), in the plasma sheet. cf. Kronberg et al., 2009.

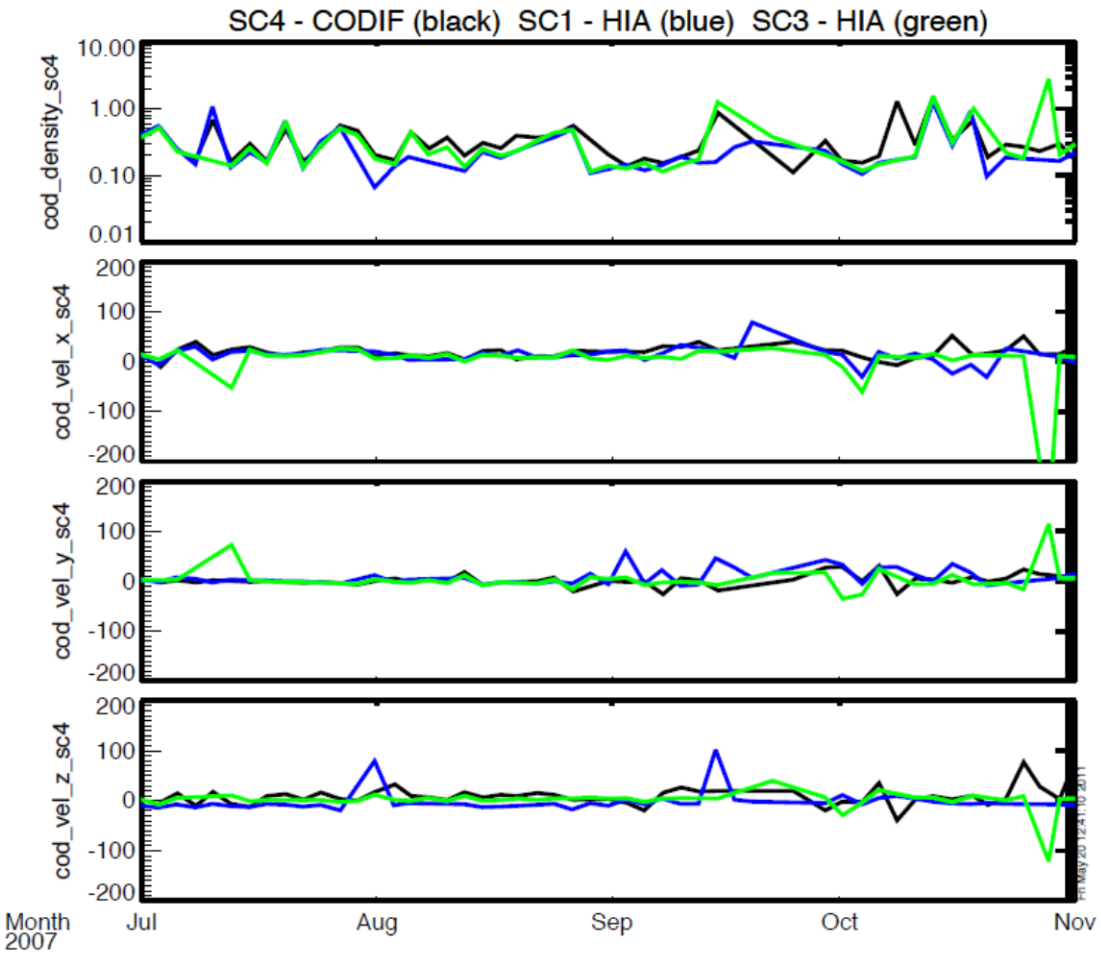

Figure 6.7

CODIF-HIA densities and velocities comparisons: average densities and velocities in the plasma sheet from CODIF, on Cluster 4, and from HIA on Cluster 1 and Cluster 3. cf. Kistler et al., 2013.